

Efficiency of dye-sensitized solar cells based on TiO₂ nanoparticle/nanowire composites

Hyukjae Lee^a, Jin-Il Park^b, Tae-Heui Kim^b and Kyung-Bong Park^{b,*}

^aMaterials Research Center for Energy and Green Technology, Andong National University, Andong, Gyungbuk 760-745, South Korea

^bSchool of Materials Science and Engineering, Andong National University Andong, Gyungbuk 760-745, South Korea

TiO₂ nanoparticles and nanowires were synthesized via a hydrothermal process and used to prepare composite photoanodes for dye-sensitized solar cells. The TiO₂ nanoparticles had anatase and rutile phases, while the TiO₂ nanowires existed in the TiO₂(B), anatase, or rutile phase, depending on the post-calcination temperature. Measurement of the photovoltaic performance by a solar simulator showed that the composite photoanodes prepared from TiO₂ nanoparticles and nanowires displayed superior light-to-electricity conversion efficiencies compared to those made solely of nanoparticles or of nanowires. Furthermore, all anatase-phase TiO₂ nanoparticle/nanowire composites gave higher conversion efficiencies than did anatase nanoparticle/TiO₂(B) nanowire composites. The highest conversion efficiency was found for the composite photoanode made of 90 wt% anatase TiO₂ nanoparticles and 10 wt% anatase TiO₂ nanowires.

Key words: Anatase, TiO₂(B), Nanoparticles, Nanowires, Dye-sensitized solar cell.

Introduction

Dye-sensitized solar cells (DSSCs) have attracted intense scientific attention because of their advantages over conventional Si-based devices, such as flexibility, low cost, light weight, and the low toxicity of the manufacturing process [1, 2]. DSSCs are typically made of two transparent conducting glasses, one of which is a photoanode [3–6] and the other is a counter electrode, with an iodide electrolyte between the electrodes. TiO₂ has traditionally been the primary material for the photoanode. At the photoanode, light absorption by dye molecules results in the injection of electrons into the conduction band of the porous TiO₂. The excited dye is then restored to its original state by electron donation from the reducing ions present in the electrolyte, which in turn are reduced at the counter electrode [7]. In conventional DSSCs that employ nanoparticulate TiO₂, the electrons diffuse to the anode by “hopping” from particle to particle, and each hop may lead to recombination with the electrolyte, thus limiting the light-to-electricity conversion efficiency of DSSCs [8, 9]. In contrast, one-dimensional nanostructures such as nanorods, nanowires, and nanotubes can provide a direct path to the current-collecting electrode and can increase the diffusion rate without raising the recombination rate, thus enhancing the conversion efficiency of DSSC. Unfortunately, one-dimensional TiO₂ nanostructures have a relatively low specific surface area, crystallinity, and substrate adhesion

strength compared to nanoparticulate TiO₂, which may adversely affect the photovoltaic performance [10, 11]. It may be expected, however, that composite TiO₂ photoelectrodes composed of nanoparticles and one-dimensional nanostructures show the combined merits of the two approaches. Indeed, several previous studies have shown an enhancement in the conversion efficiency for composite TiO₂ photoanodes [12–15].

Although TiO₂ has several polymorphs, most studies concerning the application of composites of TiO₂ nanoparticles and one-dimensional nanostructures in DSSCs have focused on anatase TiO₂ [12–15]. The present study is part of an effort to understand the effect of the nature of the TiO₂ phase on the photovoltaic performance of TiO₂ nanostructure-based DSSCs. First, anatase- or TiO₂(B)-phase nanoparticles and nanowires were synthesized using hydrothermal methods, and composite photoanodes were then prepared with different weight ratios of nanoparticles and nanowires. Finally, the material properties and photovoltaic performance of the composite photoanodes were systematically investigated in order to determine the effect of the TiO₂ phase on the conversion efficiency of the composite photoanode.

Experimental Procedure

Synthesis of TiO₂ nanoparticles and nanowires

TiO₂ nanoparticles were prepared by a sol-gel process, followed by hydrothermal treatment. First, triethylamine (TEA, 98%, Aldrich) was added to de-ionized water, and the mixture was stirred for 30 min in a Teflon-lined autoclave. Then, titanium isopropoxide (TIP, 97%, Aldrich) was slowly added with the H₂O/TIP (R) ratio of 100. After vigorous stirring at 80 °C

*Corresponding author:
Tel : 82-54-820-5427
Fax: 82-54-820-6211
E-mail: kbpark@andong.ac.kr

for 3 hrs, hydrothermal treatment was conducted for another 6 hrs at 180 °C to grow the TiO₂ nanoparticles. The resulting solution was washed several times with ethanol and distilled water, and then centrifuged at 3000 rpm for 3 min to obtain white precipitates. The precipitates were dried at 100 °C for 24 hrs.

TiO₂ nanowires were prepared by the hydrothermal reaction of synthesized TiO₂ powders in aqueous NaOH solution. TiO₂ powders (10 g) with an average particle diameter of 20 nm were added to a NaOH solution (1 L, 10 M) and then stirred for 2 hrs at room temperature. The solution was transferred to an autoclave and heat-treated at 150 °C for 72 hrs. After cooling, the precipitate was collected and washed with distilled water. For ion exchange of Na⁺ with H⁺, the precipitates were stirred for 24 hrs in HCl solution (0.05 M) and washed again with distilled water until the pH was ~7. The resulting powder was dried at 100 °C for 24 hrs and then calcined for 2 hrs at the temperatures specified below.

Characterization and measurement

The thermophysical properties of TiO₂ nanoparticles and nanowires were determined using a thermal analyzer system (Setaram TG-DTA/DSC), under a N₂ atmosphere. The phase and crystallinity of the TiO₂ nanoparticles and nanowires was investigated by X-ray diffraction (XRD, Rigaku D/MAX 2000 with Cu K α radiation), while the morphologies were examined using a field emission scanning electron microscope (FE-SEM, JEOL JSM-6700F) and a transmission electron microscope (TEM, JEOL JEM-2010). For the calculation of the specific surface area, nitrogen adsorption and desorption measurements were carried out using a Micromeritics ASAP-2010.

The TiO₂ composite paste was prepared from nanoparticles containing 0, 10, 15, or 100 wt% nanowires, ethyl cellulose binder (45CP, Kanto Chemical), and α -terpineol solvent (Kanto Chemical) in a weight ratio of 18:9:73. The TiO₂ composite paste was then coated onto fluorine-tin-oxide (FTO) glass (Solaronix) by the screen printing technique. After pre-cleaning the FTO glass, the screen printing of the TiO₂ composite paste was conducted several times to obtain the desired thickness. Between each print, the FTO glass was heat treated at 450 °C for 30 min. The screen-printed FTO glass was used as a working electrode in DSSC after immersion in an N719 dye solution for 6 h and subsequent aging in a dark room for 24 hrs. Pt-coated FTO glass, which was heat-treated at 450 °C for 30 min after coating, was used as a counter electrode. The electrolyte consisted of iodine (Aldrich) and lithium iodide (Aldrich) in a mixture of acetonitrile (Junsei) and 4-*tert*-butylpyridine (Aldrich). The current density-voltage (J-V) curves of the DSSCs were measured using a solar simulator under AM 1.5 illumination conditions.

Results and Discussion

In Fig. 1(a), the differential thermal analysis (DTA) curve of the as-synthesized TiO₂ nanoparticles shows a weak endothermic peak at 100 °C owing to the desorption of water molecules from the particle surface. Likewise, the thermogravimetry (TG) curve shows weight loss above 100 °C because of the evaporation of adsorbed water. The exothermic peaks at 240 °C are likely associated with the combustion of C-H organic residues in the TiO₂ nanoparticles, while at 700 °C, phase transition from the anatase to the rutile phase occurs. XRD patterns of TiO₂ nanoparticles after 2 hrs heat treatment at temperatures varying from 300 to 800 °C are shown in Fig. 2. The pure anatase phase is observed until 600 °C, while mixed phases of anatase and rutile appear at temperatures above 700 °C. This phase transition from anatase to rutile at 700 °C is in agreement with the DTA result. Fig. 3 shows the XRD patterns of TiO₂ nanowires calcined at different temperatures. The XRD pattern of as-synthesized nanowires, i.e., before calcination, matches that of H₂Ti₃O₇. Between a calcination temperature of 300 and 500 °C, thermal dehydration of H₂Ti₃O₇ leads to the formation of the TiO₂(B) phase. Further heating results in the transformation to the anatase phase at 600 °C, while mixed phases of anatase and rutile appear at a calcination temperature of 700 °C, which is similar to

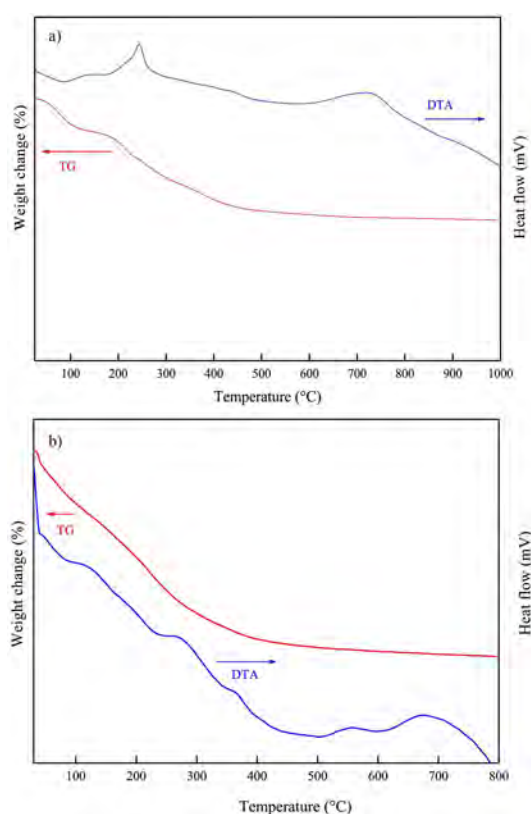


Fig. 1. TG-DTA curves of as-synthesized TiO₂ nanoparticles (a) and nanowires (b). Heating rate is 10 °C/min.

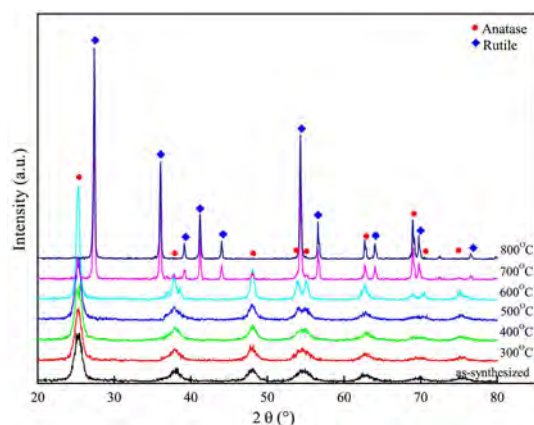


Fig. 2. XRD patterns of TiO₂ nanoparticles heat-treated at 300–800 °C for 2 h.

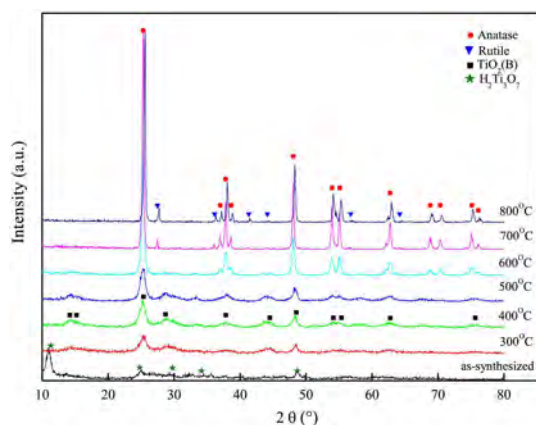


Fig. 3. XRD patterns of TiO₂ nanowires calcined at 300–800 °C for 2 h.

the case of the TiO₂ nanoparticles (Fig. 2). The DTA curve of the as-synthesized TiO₂ nanowires (Fig. 1(b)) shows several peaks arising from the various processes that occur during heat treatment, such as dehydration, formation of TiO₂(B) (between 250 and 380 °C), transformation into the anatase phase at ~560 °C, and transformation into the rutile phase at ~680 °C.

SEM and TEM images of the as-synthesized TiO₂ nanoparticles (Figs. 4(a) and 4(b), respectively) show anatase-phase nanoparticles in the 20–30 nm size range. The as-synthesized H₂Ti₃O₇ nanowires shown in Fig. 4c are several micrometers long and 20–50 nm in diameter. Several nanowires are fused together and they form a bundle with a width of around 200 nm. High-temperature calcination of the as-synthesized H₂Ti₃O₇ nanowires led to the dehydration and growth of nanowires. As the calcination temperature increases, the nanowire diameter increases and the nanowire surface becomes smoother and more rounded (Fig. 5). This smooth and rounded nanowire surface is shown in more detail in Fig. 6. The electron diffraction patterns (Fig. 6, inset) show the two different TiO₂ phases obtained at different calcination temperatures, i.e., TiO₂(B) at 400 °C and anatase at 600 °C. Brunauer-

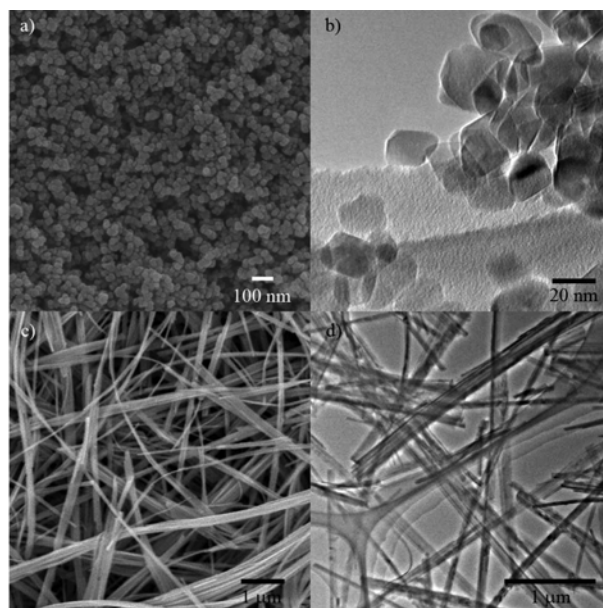


Fig. 4. SEM and TEM images of as-synthesized TiO₂ nanoparticles (a, b) and TiO₂ nanowires (c, d).

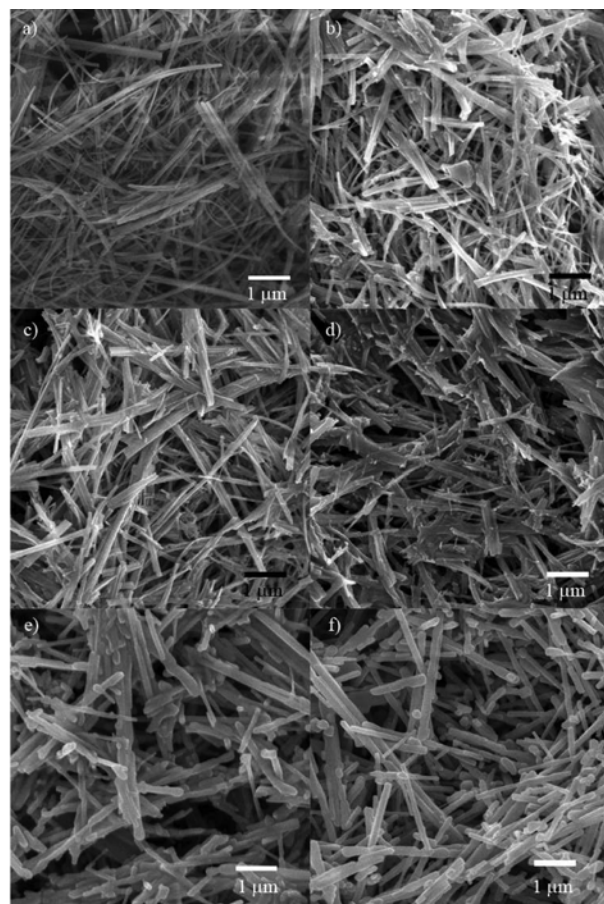


Fig. 5. SEM images of TiO₂ nanowires calcined for 2 h at different temperatures. (a) 300 °C, (b) 400 °C, (c) 500 °C, (d) 600 °C, (e) 700 °C, (f) 800 °C.

Emmett-Teller (BET) surface areas calculated from the N₂ adsorption and desorption isotherms for as-synthesized

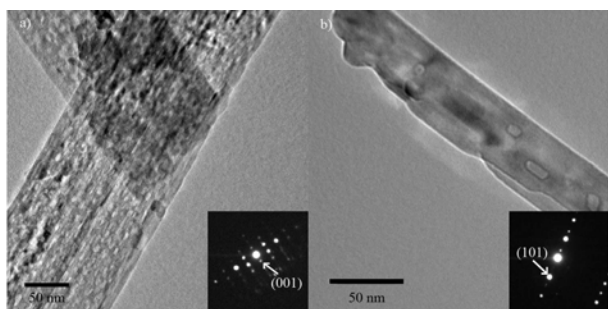


Fig. 6. TEM images of TiO₂ nanowires calcined at (a) 400 and (b) 600 °C for 2 h.

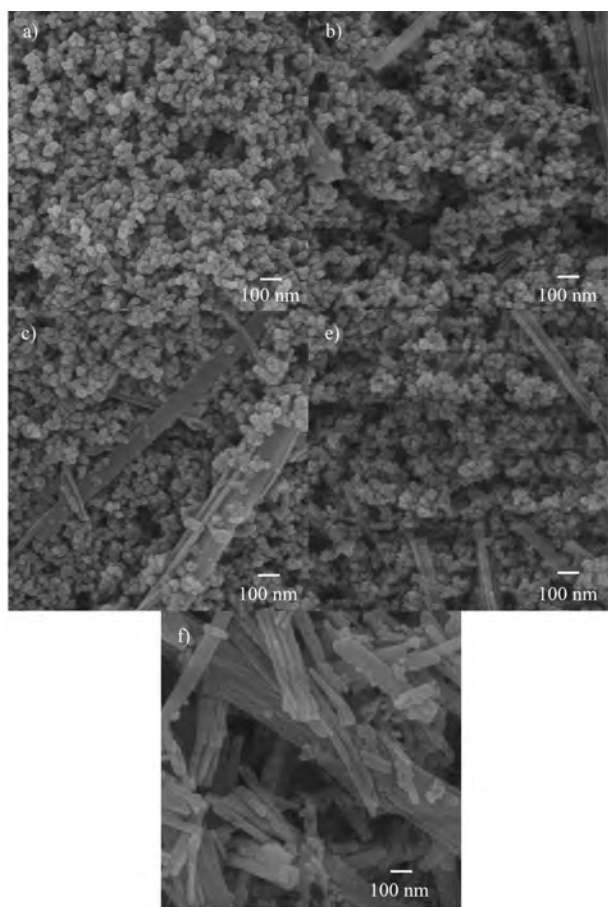


Fig. 7. SEM images of Type A composite photoanodes with different wt% of TiO₂ nanowires. (a) 0 wt%, (b) 10 wt%, (c) 15 wt%, (d) 20 wt%, (e) 100 wt%.

H₂Ti₃O₇ nanowires, TiO₂ nanowires calcined at 400 °C, and TiO₂ nanowires calcined at 600 °C were 146, 81, and 39 m² g⁻¹, respectively. Apparently, because of the growth of the nanowires, the BET surface area decreases as the calcination temperature increases. The reduced surface area at high calcination temperatures can have an adverse effect on the photovoltaic performance because the number of dye molecules and nanoparticles that can adsorb/attach to the nanowire surface is lower.

Two types of composite photoanodes were prepared

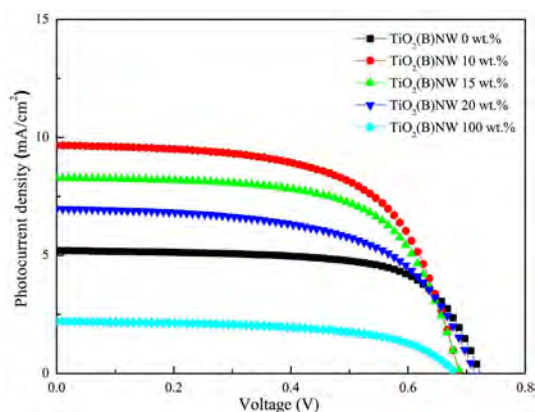


Fig. 8. Current density versus voltage (J-V) curves of DSSCs made of Type A photoanodes.

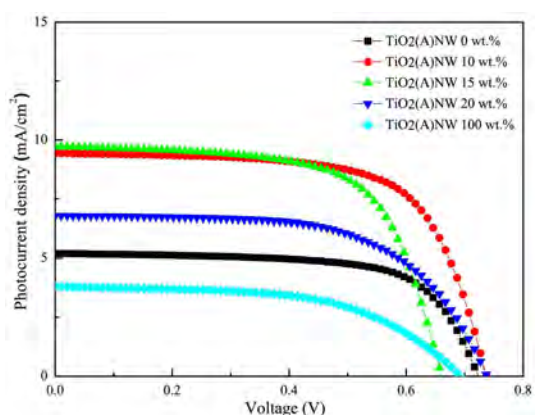


Fig. 9. Current density versus voltage (J-V) curves of DSSCs made of Type B photoanodes.

by the addition of 0, 10, 15, 20, and 100 wt% TiO₂ nanowires—calcined at either 400 °C (Type A) or 600 °C (Type B)—to the anatase TiO₂ nanoparticles. It should be noted that TiO₂ nanowires calcined at 400 and 600 °C have TiO₂(B) and anatase phases, respectively. In SEM images of Type A photoanodes (Fig. 7), smooth and well-dispersed composite layers are observed on the FTO glass, except for the photoanode prepared solely from TiO₂ nanowires (Fig. 7(f)), where the large size and extremely high aspect ratio of the nanowires results in poor contacts between the wires. Type B photoanodes showed similar features (data not shown).

J-V curves of DSSCs made from Type A and Type B photoanodes are shown in Figs. 8 and 9, respectively, while Tables 1 and 2 summarize the open-circuit voltages, short-circuit current densities, fill factors, and conversion efficiencies. The highest conversion efficiencies were found for the composite photoanodes prepared from 90 wt% TiO₂ nanoparticles and 10 wt% TiO₂ nanowires, both for Type A (3.8%) and Type B (4.5%) photoanodes. It is postulated that the addition of nanowires to the nanoparticles provides a fast route for electron transport, and since the nanoparticles are relatively small, they show good contact with the nanowires and good

Table 1. Photovoltaic parameters of DSSCs Made of Type A photoanodes.

Wt% of TiO ₂ nanowires (%)	Open Circuit Voltage (V)	Current Density (mA/cm ²)	Fill Factor (%)	Conversion Efficiency (%)
0	0.72	5.2	0.67	2.5
10	0.68	9.7	0.57	3.8
15	0.68	8.3	0.62	3.5
20	0.70	7.0	0.56	2.8
100	0.67	2.2	0.55	0.82

Table 2. Photovoltaic parameters of DSSCs Made of Type B photoanodes.

Wt% of TiO ₂ nanowires (%)	Open Circuit Voltage (V)	Current Density (mA/cm ²)	Fill Factor (%)	Conversion Efficiency (%)
0	0.72	5.2	0.67	2.5
10	0.73	9.4	0.65	4.5
15	0.66	9.8	0.63	4.1
20	0.73	6.8	0.64	3.2
100	0.67	3.8	0.49	1.2

adhesion to the substrate, resulting in the higher conversion efficiency. In contrast, photoanodes made of pure TiO₂ nanowires show very low conversion efficiencies, i.e., 0.82% for Type A and 1.2% for Type B anodes, which could result from poor contacts between the nanowires, as shown in Fig. 7. Type B photoanodes show an enhanced photovoltaic performances compared to Type A anodes under all conditions. Considering that Type A photoanodes are two-phase composites (TiO₂(B) and anatase), the inferior photovoltaic performances of Type A composite photoanodes might be caused by the electrical and physical discontinuities between the nanowires and nanoparticles. In addition, the decreased crystallinity of the TiO₂(B) phase compared to the anatase phase (Fig. 3) may be a factor.

Although all anatase-phase nanoparticle/nanowire composites showed an increased photovoltaic performance in the present study, further investigation is needed to fully understand the effect of the different TiO₂ phases on the photovoltaic performance. For instance, all TiO₂(B)-phase nanoparticle/nanowires composites may yield interesting results since the TiO₂(B) phase is known to contain a more open structure than the anatase phase and could therefore facilitate faster electron transport [16]. In addition, further modification of the TiO₂ nanoparticles and nanowires and/or the optimization of the synthesis procedures can boost the photovoltaic performance to a greater extent.

Conclusions

TiO₂ nanoparticles and nanowires were prepared via a hydrothermal process and used to prepare composite photoanodes for DSSCs. Depending on the post-calcination temperatures, the TiO₂ nanoparticles and nanowires existed in the TiO₂(B), anatase, or rutile phase. The TiO₂ photoanodes made of nanoparticle/nanowire composites showed an enhanced photovoltaic performance compared to those prepared solely from nanoparticles or nanowires. In addition, anatase-phase TiO₂ nanoparticle/nanowire composites showed higher conversion efficiencies than did anatase nanoparticle/TiO₂(B) nanowire composites. The highest conversion efficiency was found for the composite photoanode prepared from 90 wt% anatase TiO₂ nanoparticles and 10 wt% anatase TiO₂ nanowires.

Acknowledgments

This work was supported by a grant from 2012 Research Fund of Andong National University.

References

1. B. Oregan and M. Gratzel, *Nature* 353 (1991) 737-740.
2. M. Gratzel, *J. Sol-Gel Sci. Technol* 22 (2001) 7-13.
3. M. Wei, Y. Konishi, H. Zhou, M. Yanagida, H. Sugihara, and H. J. Arakawa, *J. Mater. Chem.* 16 (2006) 1287-1293.
4. Y.J. Kim, M.H. Lee, H.J. Kim, G. Lim, Y.S. Choi, N.G. Park, K. Kim, and W.I. Lee, *Adv. Mater.* 21 (2009) 3668-3673.
5. K. Zhu, N.R. Neale, A. Miedaner, and A.J. Frank, *Nano Lett.* 7 (2007) 69-74.
6. D. Chen, F. Huang, Y.B. Cheng, and R.A. Caruso, *Adv. Mater.* 21 (2009) 2206-2210.
7. U. Bach, D. Lupo, P. Comte, J.E. Moser, F.W. Ortel, J. Salbeck, H. Spreitzer, and M. Gratzel, *Nature* 395 (1998) 583-585.
8. J.B. Baxter, A. Walker, K. Ommering, and E. Aydil, *Nanotechnol.* 17 (2006) S304-S312.
9. Y. Tachibana, J.E. Moser, M. Gratzel, D.R. Klug, and J.R. Durrant, *J. Phys. Chem.* 100 (1996) 20056-20062.
10. J.T. Jiu, S. Isoda, F.M. Wang, and M. Adachi, *J. Phys. Chem. B* 110 (2006) 2087-2092.
11. M. Adachi, Y. Murata, J. Takao, J.T. Jiu, M. Sakamoto, and F.M. Wang, *J. Am. Chem. Soc.* 126 (2004) 14943-14949.
12. B. Tan and Y. Wu, *J. Phys. Chem. B* 110 (2006) 15932-15938.
13. K.M. Lee, V. Suryanarayanan, J.H. Huang, K.R.J. Thomas, J.T. Lin, and K.C. Ho, *Electrochim. Acta* 54 (2009) 4123-4130.
14. Y. Alivov and Z.Y. Fan, *Appl. Phys. Lett.* 95 (2009) 63504-63506.
15. P. Roy, D. Kim, I. Paramasivam, and P. Schmuki, *Electrochem. Commun.* 11 (2009) 1001-1004.
16. A.R. Armstrong, G. Armstrong, J. Canales, and P.G. Bruce, *Angew. Chem., Int. Ed.* 43 (2004) 2286-2288.